CHEMISTRY OF MATERIALS

Article

pubs.acs.org/cm

Intrinsic Conductivity in Magnesium–Oxygen Battery Discharge Products: MgO and MgO_2

Jeffrey G. Smith,[†] Junichi Naruse,[§] Hidehiko Hiramatsu,[∥] and Donald J. Siegel*[,†,#,▽,‡,⊥]

[†]Mechanical Engineering Department, [▽]Materials Science & Engineering, [‡]Applied Physics Program, and [#]Michigan Energy Institute, University of Michigan, Ann Arbor, Michigan 48109, United States

[§]North America Research & Development, DENSO International America, Inc., 24777 Denso Drive, Southfield, Michigan 48086, United States

[∥]Research Laboratories, DENSO Corporation, 500-1, Minamiyama, Komenoki-cho, Nisshin, Aichi 470-0111, Japan

[⊥]Department of Energy Conversion and Storage, Technical University of Denmark, Fysikvej, Building 309, 2800 Kongens Lyngby, Denmark

ABSTRACT: Nonaqueous magnesium–oxygen (or "Mg-air") batteries are attractive next generation energy storage devices due to their high theoretical energy densities, projected low cost, and potential for rechargeability. Prior experiments identified magnesium oxide, MgO, and magnesium peroxide, MgO_2, as the primary discharge products in a Mg/O_2 cell. Charge transport within these nominally insulating compounds is expected to limit battery performance; nevertheless, these transport mechanisms either are incompletely understood (in MgO_2) or remain a matter of debate (in MgO). The present study characterizes the equilibrium conductivity associated with intrinsic (point) defects within both compounds using first-principles calculations. For MgO, negative Mg vacancies and hole polarons—the latter localized on oxygen anions—were identified as the dominant charge carriers. However, the large formation energies associated with these carriers suggest low equilibrium concentrations. A large asymmetry in the carrier mobility is predicted: hole polarons are highly mobile at room temperature, while Mg vacancies are essentially immobile. Accounting for nonequilibrium effects such as frozen-in defects, the calculated conductivity data for MgO is shown to be in remarkable agreement with the three "Arrhenius branches" observed in experiments, thus clarifying the long-debated transport mechanisms within these regimes. In the case of MgO_2, electronic charge carriers alone—electron and hole polarons—are the most prevalent. Similar to MgO, the equilibrium concentration of carriers in MgO_2 is low, and moderate-to-poor mobility further limits conductivity. If equilibrium behavior is realized, then we conclude that (i) sluggish charge transport in MgO or MgO_2 will limit battery performance when these compounds cover the cathode support and (ii) what little conductivity exists in these phases is primarily electronic in nature (i.e., polaron hopping). Artificially increasing the carrier concentration via monovalent substitutions is suggested as a strategy for overcoming transport limitations.

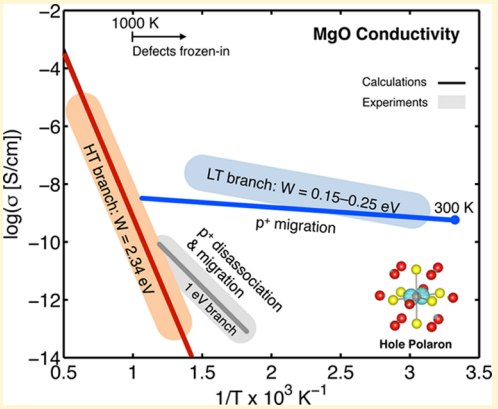

I. INTRODUCTION

The demand for energy-dense batteries suitable for electric vehicle propulsion has sparked interest in metal–oxygen electrochemistry. For example, a rechargeable battery based on a multivalent Mg/O_2 couple that discharges to magnesium oxide has a theoretical energy density that is nearly seven times (3.9 kW h/kg) that of conventional Li-ion batteries (0.57 kW h/kg) and even surpasses that of a "Li–air" cell (3.5 kW h/kg, assuming discharge to Li_2O_2).[1−5] Additional advantages of magnesium-based systems compared to Li analogues include an anode with higher volumetric capacity (3832 mA h cm^{-3} Mg vs 2062 mA h cm^{-3} Li), suppressed dendrite formation, and lower cost.[6,7]

As a result of the nearly identical formation energies of magnesium oxide, $\Delta G_f^0(MgO) = -568.9$ kJ/mol,[8] and magnesium peroxide, $\Delta G_f^0(MgO_2) = -567.8$ kJ/mol,[9] both compounds may be expected to participate in the cycling of nonaqueous Mg/O_2 cells. By analogy with Li–air cells that reversibly cycle Li_2O_2, these MgO_x compounds could appear as a solid discharge product within the cathode during discharge and subsequently decompose during charging, according to

$$Mg^{2+} + 2e^- + \frac{1}{2}O_2 \rightleftharpoons MgO,\ U_0 = 2.95\ V \quad (1)$$

$$Mg^{2+} + 2e^- + O_2 \rightleftharpoons MgO_2,\ U_0 = 2.94\ V \quad (2)$$

Mg/O_2 batteries using nonaqueous electrolytes have recently been reported.[10−13] In the experiments performed by Shiga et al. it was concluded that the discharge product was MgO; furthermore, it was demonstrated that MgO was not

Received: January 17, 2017
Revised: March 8, 2017
Published: March 8, 2017

DOI: 10.1021/acs.chemmater.7b00217
Chem. Mater. XXXX, XXX, XXX−XXX

rechargeable at moderate voltages unless a redox mediator was present.[10,11] In a later study employing a different electrolyte, Vardar et al. found the discharge product to comprise a mixture of MgO and MgO_2, with the peroxide component exhibiting more facile decomposition during recharge.[12] In agreement with these experimental observations, ab initio calculations of the theoretical limiting voltage in Mg/O_2 batteries predicted low voltaic efficiency (~30%) for cells that cycle MgO. In contrast, cells that discharge to MgO_2 were predicted to achieve much higher efficiencies, up to approximately 90%.[9]

To realize high energy densities it is desirable to maximize the quantity of the MgO_x discharge product formed within the cathode (i.e., maximize discharge capacity). Unfortunately, maximizing capacity is likely at odds with achieving efficient battery operation, as "sudden death" and high charging voltages in analogous Li/O_2 batteries have both been attributed to the insulating nature of the discharge product.[1,4,14−20] In these systems lithium peroxide (Li_2O_2) forms on the cathode during discharge, impeding charge migration from the cathode support to the electrolyte/Li_2O_2 interface. One may speculate that sluggish charge transport through the discharge product is a universal limitation that must be circumvented to cycle any metal−oxygen battery at high capacity, regardless of the anode composition. These considerations suggest that understanding transport mechanisms in metal−oxygen compounds—including oxides, peroxides, and superoxides—is a prerequisite for the rational design of efficient metal−air batteries.

In the case of MgO, most experimental measurements of transport have been conducted at temperatures exceeding 1000 K.[21−32] Of course, for battery applications it is the low-temperature conductivity that is most relevant. The paucity of measurements near room temperature is presumably due to difficulties associated with measuring the (very low) conductivity of nominally insulating MgO. These measurements are further compounded by the presence of impurities, variations in sample preparation, and sensitivity to the temperature history of the sample, the latter being indicative of a failure to achieve equilibrium at low temperatures.[31,32]

Despite these complications, clear trends in the experimental data for MgO have emerged. Most notable among these is the observation of three distinct "Arrhenius branches" associated with the conductivity as a function of temperature.[33] The conductivity is conventionally described in terms of the Arrhenius energy, W, according to the expression $\sigma = \sigma_0 \exp(-W/k_BT)$. Here W is the sum $(E_f + E_b)$ of the formation and migration energies of a particular charge carrier. Unusually, the conductivity data for MgO exhibits three distinct W values of approximately 2.4, 1, and 0.2 eV.[21,31−33] These differing values suggest the transport mechanism in MgO varies as a function of temperature. Although speculation regarding the different mechanisms has been offered,[32−35] little direct evidence exists.

Transport in MgO has also been studied using a variety of computational methods. These studies typically focus on intrinsic ionic (point) defects such as vacancy-interstitial pairs (i.e., Frenkel defects) or vacancies involving both cations and anions (i.e., Schottky defects). Early calculations from Catlow[36] and Mackrodt[37,38] using model potentials found that the formation energies were large for both Schottky (~7 eV) and Frenkel (~12−15 eV) defects, precluding any sizable concentration. Subsequent studies[39−49] have reaffirmed these high formation energies using more sophisticated methods that range from first-principles DFT[41,46−48] to quantum Monte Carlo.[44] In contrast to the large number of studies on Schottky and Frenkel defects in MgO, little effort has been devoted to characterizing electronic carriers such as polarons.

Although a large number of studies have been conducted on MgO, charge transport in alkaline earth peroxides such as MgO_2 is essentially unexplored. This also differs from the situation for alkali metal peroxides and superoxides, such as Li_2O_2, sodium peroxide (Na_2O_2), and sodium superoxide (NaO_2),[14,15,50−59] for which a number of studies have recently appeared. In the case of Li_2O_2, experiments and calculations agree on the identity of the charge carriers as negative Li vacancies and positive hole polarons, although there is some discrepancy in the magnitude of the conductivity.[15,52] Calculations on these compounds predict low electronic conductivities in the range of approximately 10^{-20} to 10^{-19} S/cm.[15,56] Likewise, ionic conductivity was also predicted to be low in the peroxides—10^{-19} S/cm in Li_2O_2 and Na_2O_2—and several orders of magnitude higher, 10^{-10} S/cm, for the superoxide NaO_2.[15,56] Regarding experiments, the electrical conductivity of Li_2O_2 at 100 °C was measured at 10^{-12} to 10^{-11} S/cm.[52] Measurements on the alkali−metal superoxides (KO_2, RbO_2, and CsO_2) reported values in the same range as for Li_2O_2.[57] The difference between theory and experiment can arise from the presence of impurities or from nonequilibrium defect concentrations.[60−62] The latter effect results in higher-than-expected concentrations at low temperatures, due to the freeze-in of defects upon cooling of the sample.[61] To put these values in context, the electrical conductivity of common Li-ion cathode materials falls in the range of 10^{-5} to 10^{-9} S/cm.[63]

In the present study ab initio calculations at the hybrid level of theory and beyond (GW method) are employed to identify the concentrations and mobilities of intrinsic (point) defects in MgO and MgO_2. In so doing, we shed light on potential performance limitations in Mg/O_2 batteries arising from sluggish transport through these phases. In addition, a comparison between our calculations and the experimental literature allow us to clarify the elusive conduction mechanisms associated with the three Arrhenius branches observed for MgO. Formation energies and concentrations are calculated for several varieties of vacancies, interstitials, and polarons. Subsequently, the mobility of the dominant (i.e., highest-concentration) defects are calculated with the nudged elastic band method.[64−66] The resulting conductivity data are compared to that of the discharge products of other metal−oxygen systems, namely, Li/O_2 and Na/O_2.

Many-body perturbation theory calculations performed at the GW level of theory reveal MgO and MgO_2 to be insulators with large bandgaps approaching 8 eV. For MgO we find the dominant point defects to be hole polarons localized on the oxygen sublattice and negative Mg vacancies (V_{Mg}^{2-}) with a formal charge of −2. The formation energy for both defects is high, 2.2 eV, indicative of low concentrations. The calculated mobility of V_{Mg}^{2-}, 4×10^{-38} $cm^2/(V\ s)$, is very low, but in excellent agreement with experimental data, 1.5×10^{-37} $cm^2/(V\ s)$.[29] In contrast, the mobility of hole polarons is much higher, 6×10^{-3} $cm^2/(V\ s)$. In the case of MgO_2, electronic charge carriers alone—electron and hole polarons—are the most prevalent. Similar to MgO, the absolute concentration of carriers in MgO_2 is low, and moderate-to-poor mobility further limits conductivity.

Our calculations indicate that at room temperature the equilibrium conductivity for both MgO and MgO_2 is low (~10^{-36} S/cm), even when compared to that of other

DOI: 10.1021/acs.chemmater.7b00217
Chem. Mater. XXXX, XXX, XXX−XXX

insulating metal/O_2 discharge products such as Li_2O_2 and NaO_2. Consequently, sluggish charge transport will limit the performance of Mg/O_2 batteries by restricting the effective thicknesses and, thus, the amount of discharge product formed (i.e., capacity), during discharge. Nevertheless, the observation of moderate-to-high mobility for hole polarons in both compounds suggests a strategy for improving battery performance: artificially enhancing the hole polaron concentration via introduction of monovalent dopants.

II. METHODOLOGY

Defect formation energy and mobility calculations were performed using the Vienna ab initio simulation package (VASP code).[67−70] Blochl's projector augmented wave (PAW) method[71] was used to treat core−valence electron interactions, with valence states of 3s adopted for magnesium and 2s2p for oxygen. Many-body perturbation theory (GW method) was used to predict the bandgap of MgO and MgO_2.[72,73] The screened hybrid functional expressed with the formulation of Heyd−Scuseria−Ernzerhof (HSE)[74,75] was used with the fraction of exact exchange tuned (α = 0.42) to reproduce the bandgap from GW calculations. Finite-size energy corrections for charged systems were included via the Makov−Payne method.[76,77] The dielectric constants of MgO and MgO_2 were calculated using density functional perturbation theory;[78] values of 10.7 and 6.8 were obtained, respectively. The calculated value for MgO is in good agreement with the experimental dielectric constant, which falls in the range of 9 to 10.[35] To our knowledge the dielectric constant of MgO_2 has not been reported.

For calculations involving conventional (bulk) unit cells, the Brillouin zone was sampled with a Gamma-centered k-point mesh of density 4 × 4 × 4 for oxides/peroxides and 16 × 16 × 16 for Mg. Conventional cells were expanded into a 2 × 2 × 2 supercell for defect and mobility calculations on MgO and MgO_2. In these cases k-point sampling was performed only at the Gamma point. The plane-wave cutoff energy was set to 400 eV; all atom positions were relaxed until the forces were less than 0.04 eV/Å. The convergence criterion for electronic self-consistency was set to 10^{-6} eV. All calculations were spin polarized to account for the unpaired electron configurations preferred by some defects.

The formation energy, E_f, of a point defect X in charge state q was calculated according to the following equation:

$$E_f(X^q) = E(X^q) - E_0 - \sum_i n_i\mu_i + q\varepsilon_f + E_{MPI} \quad (3)$$

Here, E_0 represents the energy of a defect-free cell, n_i and μ_i denote the number and chemical potential of a species i that has been added to or removed from the cell in the course of creating the defect, ε_f is the Fermi level (referenced to the valence band maximum), and E_{MPI} is the Makov−Payne correction for charged systems.[76,77] Composite defects comprising more than a single point defect can also be studied with this formalism. For example, the formation energy of a Schottky defect can be evaluated by taking the sum of the energies required to form a stoichiometric defect involving vacancies on both cation and anion sites. Similarly, a Frenkel defect is evaluated as the sum of formation energies for a vacancy and an interstitial.

The chemical potential of magnesium was determined using the calculated energy, g of MgO_x (x = 1, 2) and the chemical potential of oxygen gas (μ_{O2}), $\mu_{Mg} = g_{MgOx} - (x/2)\mu_{O_2}$. Following earlier studies, corrections based on the experimental formation enthalpies were applied to both compounds to account for the combined effects of overbinding within O_2 gas and for oxidation state errors in the solid phase.[9,79]

The equilibrium concentration c of a defect can be expressed as $c = N\exp(-E_f/k_BT)$, where N is the number of (symmetry-equivalent) available defect sites per unit volume, k_B is the Boltzmann constant, and T is the absolute temperature.[80] The mobility of a defect, defined as μ, is expressed as[81]

$$\mu = \frac{\nu q a^2}{k_B T}\exp(-E_b/k_B T) \quad (4)$$

where ν is the attempt frequency (10^{13} s^{-1}) for migration,[82] q is the charge on the defect, a is the distance between neighboring defect sites, and E_b is the migration barrier. The total conductivity is expressed as a sum of the product of concentration and mobility contributions from all charge carriers i:

$$\sigma = \sum |q_i| c_i \mu_i \quad (5)$$

III. RESULTS AND DISCUSSION

Lattice Geometry. MgO adopts the rocksalt structure with an experimental lattice constant of a = 4.21 Å.[83] Vannerburg reported that MgO_2 crystallizes in the cubic pyrite structure with a lattice constant of a = 4.84 Å.[84] These crystal structures are illustrated in Figure 1. Our calculations employing the PBE-

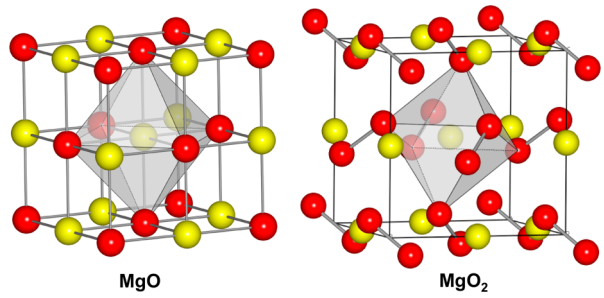

Figure 1. Crystal structure of MgO and MgO_2. Magnesium ions are octahedrally coordinated by oxygen ions in MgO and by oxygen dimers in MgO_2. Red spheres represent oxygen atoms, yellow spheres are magnesium, and the oxygen octahedron is shown in gray.

GGA functional result in a slight overprediction of the lattice constants: 4.24 Å for MgO and 4.88 Å for MgO_2.[9] On the other hand, the HSE06 functional slightly under-predicts the lattice constants: 4.19 and 4.78 Å, respectively. Consequently, we adopted the experimental lattice constants, which fall between our GGA and HSE values, for subsequent GW and defect calculations.[85]

Bandgaps. The bandgaps of MgO and MgO_2 were calculated using five different levels of theory: GGA, HSEα, non-self-consistent GW (G_0W_0), partially self-consistent GW (GW_0), and self-consistent GW (GW) methods. The GW-based methods used the GGA wave functions as input. The calculated bandgaps are summarized in Table 1. The GW_0 method has been shown to best describe the band gap of semiconductors and insulators.[85] Our calculated GW_0 value of 7.5 eV for MgO closely matches that of an earlier GW study (7.7 eV),[85] as well as the experimental band gap of ∼7.8 eV.[86] Our calculations indicate that MgO has a direct band gap at Γ, while MgO_2 has an indirect band gap. All levels of theory except the GGA predict a slightly larger bandgap for MgO_2 compared to MgO. On the basis of the GW calculations, the HSE functional was tuned to reproduce the bandgaps by mixing a fraction (α = 0.42) of exact exchange with semilocal exchange, resulting in HSEα bandgaps of 7.8 and 7.9 eV for MgO and MgO_2, respectively.

Defect Concentrations. Figure 2 shows the formation energies of 51 intrinsic defects evaluated as a function of the Fermi level for MgO and MgO_2. Five distinct charge states (−2, −1, 0, +1, and +2) were considered, with specific defect types including magnesium vacancies (blue lines), magnesium

DOI: 10.1021/acs.chemmater.7b00217
Chem. Mater. XXXX, XXX, XXX−XXX

Table 1. Calculated Band Gap for MgO and MgO_2 from Different Levels of Theory and Experimental Optical Band Gaps of MgO[86,98]

	bandgap (eV)					
	GGA	HSEα	GGA+G_0W_0	GGA+GW_0	GW	Expt.
MgO	4.5	7.8	7.1	7.5	8.2	7.4, 7.69, 7.7, 7.8
MgO (ref 85)	–	–	7.3	7.7	8.5	–
MgO_2	3.9	7.9	7.5	8.2	9.1	–

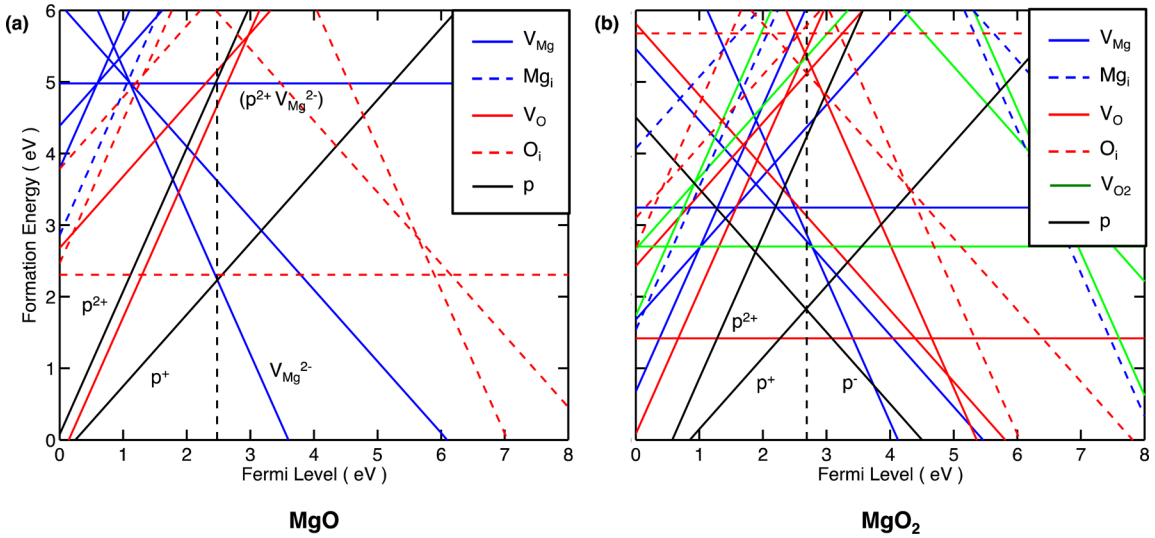

Figure 2. Formation energies of intrinsic defects in (a) MgO and (b) MgO_2 calculated using the HSEα functional. Magnesium vacancies (V_{Mg}) are depicted using blue lines, magnesium interstitials (Mg_i) with blue dashed lines, oxygen vacancies (V_O) with red lines, oxygen interstitials (O_i) with red dashed lines, and oxygen divacancies (V_{O2}) with green lines. Hole and electron polarons are shown in black. The slope of each line corresponds to its respective charge state; values of −2, −1, 0, +1, and +2 were considered. The dashed line indicates the position of the Fermi level.

interstitials (blue dashed lines), oxygen vacancies (red lines), oxygen interstitials (red dashed lines), and dioxygen vacancies (green lines); hole and electron polarons are shown in black. The slope of each line corresponds to charge state of that defect.

The vertical dashed line in Figure 2 indicates the position of the Fermi level. Under equilibrium conditions the Fermi level is set by the condition of charge neutrality, $\sum q_i c_i = 0$. This condition places the Fermi level somewhat below the center of the band gap, or 2.48 eV above the valence band maximum (VBM) for MgO and 2.69 eV above the VBM for MgO_2.

Figure 2a shows the formation energies for intrinsic defects in MgO. The defects having the lowest formation energies are the hole polaron (p^+) and magnesium vacancy (V_{Mg}^{2-}). The formation energies for these defects is high, 2.23 eV, resulting in low equilibrium concentrations for both defects of approximately 1×10^{-15} cm^{-3}. For comparison, this is many orders of magnitude less than the intrinsic carrier concentration of silicon ($\sim 10^{10}$ cm^{-3})[87] and for Li_2O_2 and Na_2O_2 ($\sim 10^7$ cm^{-3}).[15,56] The defect with the next-lowest formation energy is the neutral oxygen interstitial at 2.3 eV.

A polaron consists of a localized charge (electron or hole) and an induced local lattice distortion (i.e., polarization) in the crystal. In MgO, O^{2-} anions are octahedrally coordinated by Mg^{2+} cations with an oxygen−Mg distance of 2.1 Å. The absence of one electron on an oxygen site results in the formation of a hole polaron (p^+). The resulting oxygen ion has an electronic configuration of $2s^2 2p^5$ and a formal charge O^{1-} and hosts an unpaired electron.

The magnetization density of MgO in the vicinity of a hole polaron is illustrated in Figure 3a. The density isosurface has a shape consistent with that of an oxygen 2p orbital and is aligned along the direction where the Mg ions are furthest from the hole (d = 2.25 Å). The oxygen−Mg distance along the other

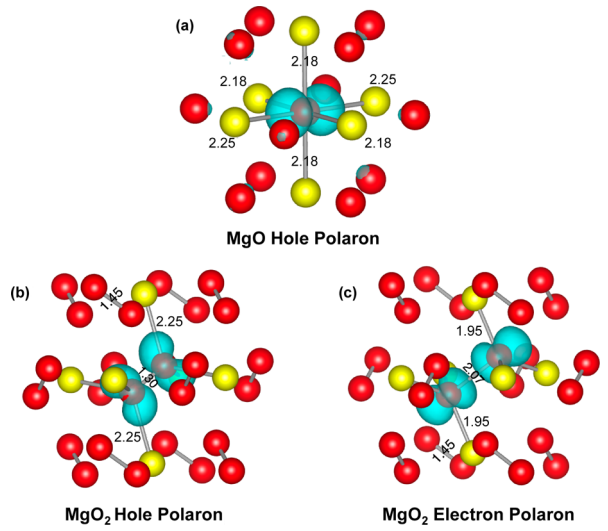

Figure 3. Magnetization density for (a) hole polaron in MgO, (b) hole polaron in MgO_2, and (c) electron polaron in MgO_2. The iso-surface is plotted at 0.01 e/Å^3. The numbers in the figure indicate bond length in Å. The oxygen to Mg bond distance in bulk is 2.1 Å for both MgO and MgO_2.

DOI: 10.1021/acs.chemmater.7b00217
Chem. Mater. XXXX, XXX, XXX−XXX

Table 2. Formation Energies and Migration Barriers for Various Defects in MgO and MgO_2[a]

	formation energy (E_f)				migration barrier (E_b)	
	Schottky	cation Frenkel	anion Frenkel	selected point defects	polaron	V_{Mg}^{2-}
MgO (this study)	6.91	10.05	13.8	2.23 (V_{Mg}^{2-} or p^+)	0.11 (p^+)	2.20
MgO (prior studies)	7.5–7.9[b], 7.5[c], 7.72[d], 8.2[e], 6.88[f], 7.53[g], 8.44[h], 7.5[i], 6.0[k], 8.8[k], 5.79[l], 5.05[m], 7.22[n] [5–7[89]]	11.9[c], 12.43[d], 13.35[h], 14.1[i], 10.3[k], 14.1[k], 10.41[m]	15.2[c], 12.33[d], 13.81[h], 13.57[j], 12.2[k], 13.6[k], 13.32[m]	–	–	1.9–2.2[b], 2.16[c], 2.07[d], 1.93[g], 2.08[h], 2.10[l], [2.28[29]]
MgO_2 (this study)	8.33	9.78	[o]10.24,[p] 12.16	1.82 (p^+ or p^-)	0.56 (p^+) 1.76 (p^-)	–

[a]Schottky and Frenkel defects are comprised of a pair of point defects; their formation energies are reported on a per pair basis. Experimental data appears in brackets. [b]Catlow et al. (1976).[36] [c]Mackrodt et al. (1979).[38] [d]Sangster et al. (1981).[39] [e]Grimes et al. (1990).[40] [f]De Vita et al. (1992).[41] [g]Vočadlo et al. (1995).[42] [h]Busker et al. (2000).[43] [i]Alfè et al. (2005).[44] [j]Uberuaga et al. (2005).[45] [k]Gilbert et al. (2007).[46] [l]Runevall et al. (2011).[47] [m]Mulroue et al. (2011).[48] [n]Grüneis (2015).[49] [o](V_O^+, O_I^-). [p](V_O^{2+}, O_I^{2-}).

two directions is elongated to a smaller degree, d = 2.18 Å, but is still larger than the bulk Mg–O nearest-neighbor distance (2.1 Å). The general elongation of these bonds relative to bulk is consistent with a weaker electrostatic interaction between the Mg^{2+} sublattice and the less-negatively charged O^{1-} (resulting from the presence of p^+). We note that the hole polaron forms only from a starting configuration wherein the symmetry of the MgO crystal is broken along one of the O–Mg bond directions. Without this distortion, the charge density relaxes to a local minimum in which the hole is delocalized. The stabilization energy for p^+, defined as the energy difference between the localized and delocalized state, is −0.24 eV. Although hole polarons can be localized on oxygen sites in MgO, we were unable to localize electrons on Mg cations.

Our prediction that doubly negative Mg vacancies, V_{Mg}^{2-}, and holes, p^+, comprise the dominant defects in MgO is consistent with experiments.[33−35,88] For example, magnetic susceptibility measurements indicate the presence of paramagnetic species in MgO,[34] a feature which could be explained by a nonzero concentration of p^+. Also, abrupt changes in the magnetic properties, charge distribution, and conductivity in MgO with respect to temperature were attributed to holes localized on the oxygen sublattice that are formed upon dissociation of a so-called "peroxy defect".[88] This composite defect is comprised of a peroxide ion (O_2^{2-}) and V_{Mg}^{2-} and is therefore neutral and nonmagnetic. Its formation energy is shown in Figure 2a as (p^{2+} V_{Mg}^{2-}).

Other defects of relevance in MgO include Schottky (a vacancy pair on anion and cation sublattices) and Frenkel (a vacancy–interstitial pair) defects, which are often present in ionic materials;[81] the formation energies of these composite defects are summarized in Table 2. Cation and anion Frenkel defects have a calculated formation energy of 10.1 and 13.8 eV, respectively, similar in magnitude to the result obtained by Mackrodt[38] (11.9 and 15.2 eV) using interatomic potentials. Regarding Schottky defects, experimental measurements of the formation energy range from 5 to 7 eV.[89] Table 2 shows our calculated Schottky defect formation energy, 6.91 eV, and a comparison with prior calculations and experiments. Our value falls near the middle of the range of calculated values,[36−49] which span 5.1–8.8 eV. A recent study[49] compared the calculated Schottky defect formation energies in MgO, as evaluated using the LDA, GGA, Hartree–Fock theory, and many electron perturbation theory. They concluded that the formation energy was within the range of 6.9 to 7.22 eV, in good agreement with our value. To our knowledge the present calculations are the first to employ a tuned hybrid functional (HSEα) to evaluate defect formation energies in MgO.

Figure 2b shows the formation energies of intrinsic defects in MgO_2. The defect with the lowest formation energy overall is the neutral oxygen vacancy. However, since this is a neutral species a contribution to charge transport is not expected. The dominant charged defects are hole (p^+) and electron polarons (p^-). The formation energies of both defects is 1.82 eV, and their concentrations are 6×10^{-9} cm^{-3}. The prediction that both charged defects in MgO_2 are electronic in nature (rather than ionic) differs from the behavior of Li- and Na-peroxide, where the lowest-energy carriers are hole polarons and negatively charged vacancies on the metal sublattice. In contrast to these other peroxides, the formation energy of a Mg cation vacancy in MgO_2 (assuming it is charge-compensated by a hole polaron) is high, 2.18 eV. An additional feature distinguishing MgO_2 from the alkali–metal peroxides is its relatively high formation energies: the most populous carriers in MgO_2 have formation energies (1.82 eV) that are approximately double those reported for Na_2O_2 and Li_2O_2.[15,56]

In MgO_2, oxygen dimers have a formal charge of 2−, i.e., O_2^{2-}, and are octahedrally coordinated by Mg^{2+} ions. The hole and electron polarons are localized on these dimers. p+ is formed by removing an electron from the dimer, resulting a half-filled π^* molecular orbital with superoxide-like character. This orbital is illustrated using magnetization density isosurfaces in Figure 3b. The shortened O–O bond distance of 1.3 Å in the presence of p^+ is consistent with the bond length in magnesium superoxide.[90] In addition, the neighboring Mg ions closest to the p^+ slightly increase their distance to the dimer to 2.25 Å. All bond lengths beyond the nearest neighbor bonds are similar to those in bulk MgO_2, 2.1 Å. The stabilization energy for p^+ is −0.84 eV.

The electron polaron is formed by adding an electron to O_2^{2-}, resulting in a half-filled σ^* molecular orbital with a single, unpaired electron. The shape of the magnetization density for p^-, shown in Figure 3c, also reflects this orbital topology. The presence of p^- increases the O–O bond length significantly, to 2.1 Å, compared to 1.45 Å in the bulk. Similarly, formation of p^- contracts the Mg–O nearest-neighbor bond distance from 2.1 to 1.95 Å. The stabilization energy for p^- is −3.4 eV.

Regarding other defect types in MgO_2, the formation energies for Schottky and Frenkel defects are displayed in Table 2. For Schottky defects, the anion is defined as the oxygen dimer (i.e., O_2^{2-}) resulting in a vacancy pair of (V_{Mg}^{2-}, V_{O2}^{2+}). The formation energy of Frenkel defects involving

DOI: 10.1021/acs.chemmater.7b00217
Chem. Mater. XXXX, XXX, XXX–XXX

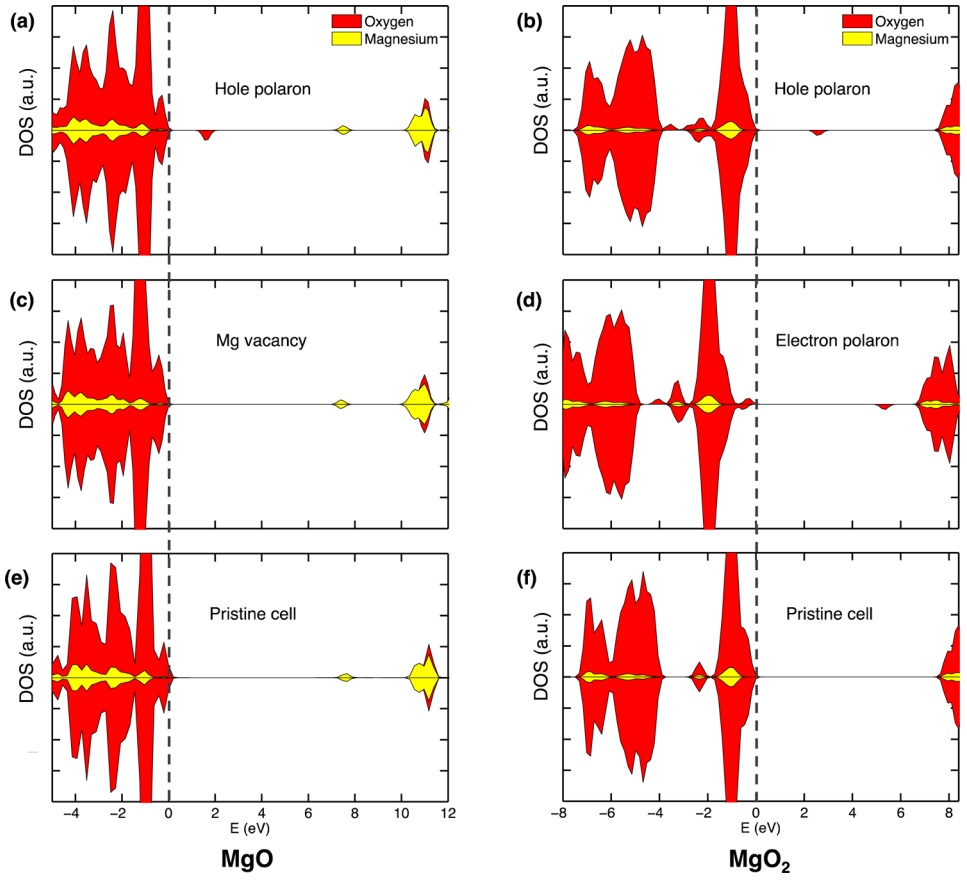

Figure 4. Density of states (DOS) calculated with the HSEα functional (α = 0.42). [Left panel] (a) Hole polaron, (c) magnesium vacancy, and (e) pristine cell in MgO. [Right panel] (b) Hole polaron, (d) electron polaron, and (f) pristine cell in MgO_2. The states above the midpoint horizontal axis are spin up, and the states below are spin down. The energies are given with respect to the top of the valence band.

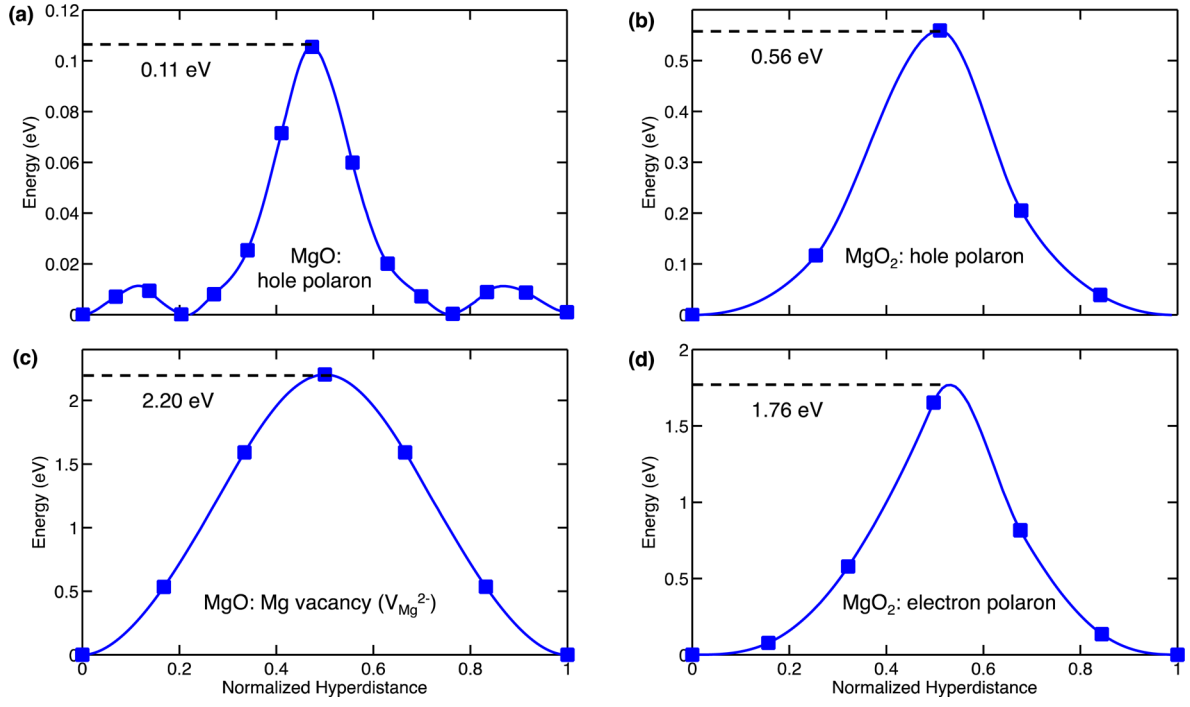

Figure 5. Migration energy barriers of dominant defects calculated using the NEB method. (a) Hole polaron and (c) magnesium vacancy (V_{Mg}^{2-}) in MgO. (b) Hole polaron and (d) electron polaron in MgO_2.

DOI: 10.1021/acs.chemmater.7b00217
Chem. Mater. XXXX, XXX, XXX−XXX

cations was evaluated as the sum of a V_{Mg}^{2-} and Mg_I^{2+}. Two types of anion Frenkel defects were considered: (V_O^{+}, O_I^{-}) and (V_O^{2+}, O_I^{2-}). As shown in Table 2, all of these defects have formation energies (~8−12 eV) similar to the analogous defects in MgO. The extremely high formation energies of all Schottky and Frenkel defects considered suggest that they will not be present in meaningful concentrations, nor will they contribute significantly to charge transport.

Electronic Structure. The density of states (DOS) for defect-free (pristine) MgO and MgO_2 are shown in Figure 4e,f, respectively. In both cases the DOS reflects the large bandgap of approximately 8 eV predicted by our GW calculations. Also, both compounds exhibit a valence band comprised of oxygen 2*p* states. The conduction band character differs, however, with MgO exhibiting primarily Mg-based states, while in MgO_2 the conduction band is comprised of σ^* orbitals on the peroxide units.

Our discussion thus far has used changes in bond lengths and magnetization densities to support the presence of polarons in MgO and MgO_2. Additional evidence can be seen in the DOS. The hole polaron in MgO (Figure 4a) and in MgO_2 (Figure 4b) introduces localized oxygen 2p states in the gap closest to the valence band maximum (VBM). These empty states emerge from the VBM upon removal of electrons from the oxygen π^* orbital during hole creation. Similarly, the electron polaron in MgO_2 (Figure 4d) introduces new 2p states near the conduction band minimum and also slightly alters the DOS just below the VBM. For comparison, the negative magnesium vacancy (V_{Mg}^{2-}) in MgO is shown in Figure 4c. In this case the DOS is mostly unchanged, indicating that the extraction of a Mg^{2+} cation has relatively minor impact on the electronic structure.

Mobility and Conductivity. The migration barriers for the highest concentration defects in MgO and MgO_2 were calculated using the nudged elastic band (NEB) method.[64−66] Both compounds possess high-symmetry (i.e., isotropic) cubic crystal structures with only one symmetry-distinct pathway for defect migration between neighboring sites. As previously mentioned, in MgO the two dominant defects are the hole polaron (p^+) and the negative Mg vacancy, V_{Mg}^{2-}. The calculated minimum energy pathway for migration of V_{Mg}^{2-} is shown in Figure 5c. This process is characterized by a high migration barrier, 2.2 eV, resulting in a low mobility of 4×10^{-38} $cm^2/(V\ s)$ at room temperature. The diffusion coefficient of V_{Mg}^{2-} is determined using the Nernst−Einstein equation, $D = \mu k_B T/q$, yielding a value of 1×10^{-39} cm^2/s, shown in Table 3. Previous computational studies of V_{Mg}^{2-} migration have reported similar activation energies in the range of 1.9 to 2.2 eV.[36,38,42,43,47,91] These values are summarized in Table 2 and agree well with the present hybrid-functional-based calculations. Our calculated activation energy and mobility for V_{Mg}^{2-} is also in good agreement with experimental measurements of Sempolinski and Kingery,[29] who reported an activation energy of 2.28 ± 0.2 eV and a mobility of 1.5×10^{-37} $cm^2/(V\ s)$ at room temperature.

In contrast to the low mobility of V_{Mg}^{2-}, hole polaron migration in MgO is relatively fast. Figure 5a plots the minimum energy pathway for p^+ migration, revealing a low barrier of 0.11 eV. Consequently, a moderately high mobility of 6.0×10^{-3} $cm^2/(V\ s)$ is predicted, along with a diffusion coefficient of 1.5×10^{-4} cm^2/s. For comparison, the mobility of holes in p-type silicon in the high doping regime is approximately 50 $cm^2/(V\ s)$.[92] We are not aware of any prior calculations or measurements of polaron mobility in MgO.

In MgO_2 our calculations predict that the dominant defects are both electronic in nature: hole (p^+) and electron (p^-) polarons. The calculated migration barriers for these carriers are shown in Figure 5b,d and demonstrate that the barrier for the migration of electron polarons is roughly three times higher (1.76 eV) than that for hole polarons, 0.56 eV. These barriers result in mobilities of 6×10^{-31} and 1×10^{-10} $cm^2/(V\ s)$, respectively. To place these values in context, in Li_2O_2 Radin et al.[15] reported in-plane and out-of-plane migration barriers for p^+ of 0.42 and 0.71 eV, respectively, using the HSEα functional. Garcia-Lastra et al.[14] found comparable barriers for p^+ of 0.39 and 0.48 eV using GGA+U. In contrast, much larger barriers were reported for migration of p^-: 1.41 and 1.47 eV. Additionally, the migration barrier for hole polaron hopping in Na_2O_2 was reported as 0.47 eV (in plane) and 0.62 eV (out-of-plane).[56] Taken together, these data suggest that in peroxides hole polarons are generally much more mobile than electron polarons, with the former exhibiting hopping barriers that are similar (~0.5 eV) regardless of peroxide composition and approximately one-third the size of p^-.

Mobilities, diffusion coefficients, and conductivity data for MgO and MgO_2 are summarized in Table 3, along with data from the literature for other alkali metal peroxides and superoxides. Under equilibrium conditions, the conductivity arising from the migration of charged point defects is the product of the carrier's charge, concentration, and mobility (eq 5). At room temperature our calculations suggest extremely low conductivities for MgO and MgO_2 of 3×10^{-36} and 3×10^{-37} S/cm, respectively. The similar conductivity of these compounds reflects a trade-off between the mobility and the concentration of the dominant carriers in these phases. In MgO hole polarons are the dominant carriers; the p^+ have high mobility but very low equilibrium concentrations. In MgO_2 this trend is reversed: p+ remain the dominant carriers, but their mobility is now lower than in MgO, yet their concentrations are proportionally higher, resulting in approximately equal conductivities.

As mentioned in the Introduction, it is nontrivial to achieve an "apples-to-apples" comparison between the calculated and measured conductivity in nominally insulating compounds at ambient temperatures. These difficulties can be traced to the presence of impurities in the sample and/or the freeze-in of nonequilibrium defect concentrations characteristic of the elevated temperatures at which the sample was prepared or conditioned.[93,94] Contributions from the sample's micro-

Table 3. Calculated Diffusion Coefficient, Mobility, and Conductivity of Dominant Defects in MgO and MgO_2[a]

compound	diffusion coefficient D (cm^2/s)	mobility μ ($cm^2/(V\ s)$)	conductivity σ (S/cm)
MgO (p^+)	1×10^{-4}	6×10^{-3}	3×10^{-36}
MgO (V_{Mg}^{2-})	1×10^{-39}	4×10^{-38}	1×10^{-71}
MgO_2 (p^+)	4×10^{-12}	1×10^{-10}	3×10^{-37}
MgO_2 (p^-)	2×10^{-32}	6×10^{-31}	7×10^{-58}
Li_2O_2 (p^+)	9×10^{-10}	–	5×10^{-20}
Na_2O_2 (p^+)	–	–	1×10^{-20}
NaO_2 (p^-)	–	–	1×10^{-19}
NaO_2 (V_{O2}^{+})	6×10^{-7}	–	4×10^{-9}

[a]Data from literature for Li_2O_2, Na_2O_2, and NaO_2 are included for comparison.[15,56]

DOI: 10.1021/acs.chemmater.7b00217
Chem. Mater. XXXX, XXX, XXX−XXX

structure may also be important. All of these effects are ignored in typical single-crystal calculations.

Literature reports have confirmed difficulties in achieving reproducible conductivity values in MgO near room temperature (RT).[21,32] These difficulties are presumably tied to the slow equilibration of charge-carrying defects.[81,93,94] For other oxides, equilibrium is typically achieved above 400−800 °C.[60] Consequently, it is not unexpected that the measured RT conductivity of MgO of ~10^{-9} S/cm[21] is significantly larger than our calculated equilibrium value of 10^{-36} S/cm. We postulate that this discrepancy is an artifact of comparing a *nonequilibrium* measurement with an *equilibrium* calculation. As described below, this explanation is bolstered by the good agreement between experiments and calculations at high temperatures, where both systems are in equilibrium.

In the case of MgO_2, it appears that conductivity measurements have not been reported. Nevertheless, we expect trends similar to those discussed above for MgO to hold for MgO_2, such as a measured (nonequilibrium) conductivity that is larger than that predicted by calculations at RT.

Of course, in a practical battery RT operation is preferred. The preceding discussion suggests that an equilibrium carrier concentration is unlikely to be achieved at this temperature. Consequently, our calculated RT conductivities should be interpreted as a lower bound to the behavior likely present in an electrochemical cell. In a realistic Mg/O_2 cell there exist two additional, potentially significant contributions to the nonequilibrium nature of the carrier concentration. The first is the rapid growth of the MgO/MgO_2 product during battery discharge. Fast discharge/growth rates should result in substantially higher defect concentrations. Second, as the growth of the discharge product occurs in an (impure) liquid electrolyte, impurities from the electrolyte may be incorporated into this product.

These two effects suggest two strategies for improving Mg/O_2 battery performance. First, since discharging at a higher rate improves the conductivity of the discharge product, performance could in principle be improved by employing pack designs that employ a larger number of reduced-capacity cells. (In these cells the effective discharge rate will be higher.) This assumes other losses due to higher-rate operation can be neglected.

A potentially more promising strategy exploits the incorporation of species from the electrolyte into the discharge product during growth. By intentionally doping the discharge product one may increase the carrier concentration. This could be achieved by substitution of aliovalent dopants on Mg sites. For example, substitution with monovalent impurities such as lithium[95,96] may increase the concentration of hole polarons, which our calculations predict are relatively mobile in both MgO and MgO_2. Assuming one polaron is created for each monovalent dopant, then a doping concentration of 10^{12} cm^{-3} (10^{19} cm^{-3}) would be needed to achieve a conductivity of 10^{-9} S/cm in MgO (MgO_2). A similar strategy has been proposed to improve the performance of Li/O_2 batteries.[17]

Explanation for the Three Arrhenius Branches in the Temperature-Dependent Conductivity of MgO. Measurements of the conductivity of solids such as MgO are conventionally presented as Arrhenius plots of the log of conductivity ($\log \sigma$) vs inverse temperature ($1/T$). The slope of the Arrhenius plot is interpreted as the "Arrhenius energy," W, which is the sum of the carrier migration barrier, E_b, as well as the carrier's formation energy, E_f ($W = E_b + E_f$):

$$\sigma(T) = \sigma_0 \exp(-W/k_B T) \quad (6)$$

Most experimental studies of conductivity in MgO focus on high temperatures above approximately 1000 K.[21−30,32] Data in this region, summarized in Figure 6, are in broad agreement

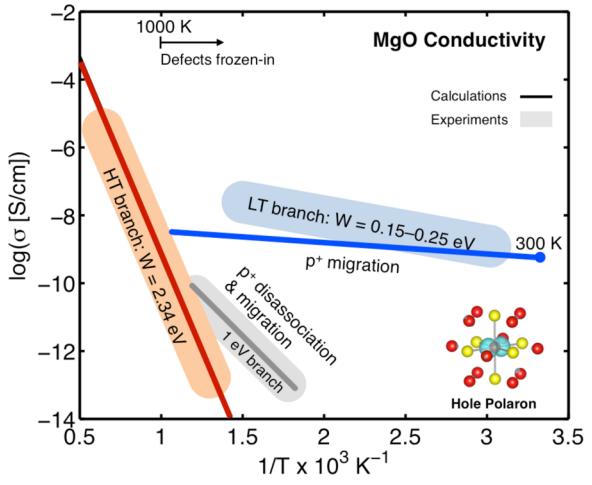

Figure 6. Arrhenius plot of the conductivity of MgO, illustrating the three Arrhenius branches reported in experiments: (red) high temperature (HT) branch, (blue) low temperature (LT) branch, and (gray) 1 eV branch.

that the Arrhenius energy is approximately 2.4 eV. Studies below 1000 K[21,32] noted that the conductivity was dependent on the temperature history of the sample; reproducible data could only be obtained during cooling after the sample was conditioned via heat treatment. At these low-to-moderate temperatures two other "Arrhenius branches" in the MgO conductivity data have been reported (Figure 6). These include a branch with a very low Arrhenius energy in the range of 0.15 to 0.25 eV[21,32] and a higher-energy branch with W = 1.0 eV.[32] Although mechanisms responsible for these branches have been proposed, direct evidence linking the measured Arrhenius energies with the identities of specific charge carriers and their respective migration mechanisms does not exist. Below we propose transport mechanisms responsible for all three Arrhenius branches using the catalogue of formation and migration energies evaluated in the present study. Before doing so, we describe the concept of "frozen in" defects in oxides.

As previously mentioned, the dearth of low-temperature conductivity data in MgO can presumably be attributed to difficulties achieving equilibrium at low temperatures. In practice, equilibrium within the crystal and between the crystal and surrounding atmosphere can be reliably obtained only at high temperatures.[93] This is because equilibrium concentrations of ionic defects are established via the transport of ions over potentially long distances, and this transport is often possible only at high temperatures. For example, the creation of a vacancy in the bulk region of a crystallite requires mass transport of ions to a "sink" such as a surface, internal void, dislocation, or grain boundary. As a crystal cools from the temperature of preparation or from an intentional heat treatment, ionic defects quickly become less mobile, and the time to achieve equilibrium increases. Consequently, defect concentrations representative of equilibrium at higher temperatures become "frozen in" with respect to the time scale over which low-temperature measurements are performed. Below these temperatures it is commonly assumed that processes

DOI: 10.1021/acs.chemmater.7b00217
Chem. Mater. XXXX, XXX, XXX−XXX

involving mass transport (i.e., ion migration) are likely to be frozen (i.e., nonequilibrated), while electronic processes such as electron transfer remain equilibrated.[81,93,97]

As described in Table 2, our calculations predict that the predominant charge carriers in MgO are (doubly) negative Mg vacancies, V_{Mg}^{2-}, and hole polarons, p^+. These carriers have identical formation energies of 2.23 eV but dramatically different activation energies for migration, E_b, of 2.20 and 0.11 eV, respectively. As shown by eq 6, the conductivity will be dominated by the carrier having the smallest Arrhenius energy, W. For an MgO crystallite in equilibrium, our calculations predict W values of 4.43 eV for V_{Mg}^{2-} and 2.34 eV for p^+. If equilibrium is not attained, for example, due to rapid cooling resulting in a frozen-in concentration of carriers, then the formation energy contribution to the Arrhenius energy can be neglected. In this case only carrier mobilites contribute to the Arrhenius energy, i.e., $W \approx E_b$.

The conductivity of MgO at high temperatures predicted using the present calculations is shown in Figure 6 with a red line. This data is compared to experimental measurements in the same temperature range, whose spread is depicted using an orange oval.[21−24,27,32] The agreement between the calculations and measurements is very good. At these high temperatures, we expect that thermal equilibrium is achieved for both p^+ and V_{Mg}^{2-}. (The calculated diffusivity for V_{Mg}^{2-}, the slower-diffusing of the two species, indicates that vacancies can traverse distances of approximately 1 μm at 1000 K over a 24-h period. This distance should be sufficient to establish equilibrium concentrations under these conditions, as diffusing ions would be capable of reaching ion sinks.) Furthermore, the experimental Arrhenius energy, W = 2.4 eV, is in remarkable agreement with the calculated value, W = 2.34 eV, assuming a hole-polaron-dominated conduction mechanism. These data indicate that the mechanism responsible for high temperature conductivity in MgO is the formation and migration of p^+. In contrast, the large Arrhenius energy (W = 4.43 eV) for ionic conductivity due to V_{Mg}^{2-} implies that vacancies have a negligible contribution to conductivity in this temperature range.

The range of experimental data[21,32] for the so-called low-temperature conductivity branch is shown in Figure 6 using a blue oval. These data were obtained by heating the sample to approximately 1000 K and recording the conductivity during cooling. The Arrhenius energy was reported to fall in the range of 0.15 to 0.25 eV. This branch can be rationalized by assuming that the concentration of charge carriers is frozen-in during the time over which measurements were performed. The presence of frozen-in defects has been noted in other oxides as well.[60,61]

To calculate a conductivity in the low-temperature regime it is necessary to adopt a value for the (nonequilibrium) carrier concentration. Given the low temperature, hole polarons, which possess a very low migration barrier of 0.11 eV, are expected to be the only mobile carriers. We assume the concentration of p^+ to be frozen-in at a value equal to their calculated equilibrium concentration (6.2×10^{11} cm^{-3}) at 1000 K. This concentration is consistent with experimental measurements[32] that suggest the freezing-in temperature for defects in MgO is near 1000 K. (Samples annealed at room temperature exhibited a continuous decrease in their conductivity, consistent with a decrease in carrier concentration, as equilibrium was slowly approached.)[31,33]

The calculated conductivity of the low-temperature (LT) branch is plotted in Figure 6 using a blue line. These calculations adopt the frozen concentration of p^+ (at 1000 K) and employ the calculated migration energy. Good agreement is obtained between the calculated and measured (blue oval) data. This agreement reflects the similar values for the Arrhenius energies—0.11 eV calculated vs 0.15 to 0.25 eV measured—and suggests that the conduction mechanism underlying the LT branch is p^+ migration alone.

A third Arrhenius branch in the MgO conductivity data is obtained when heating of the sample is interrupted at approximately 800 K.[31,32] In this case an Arrhenius energy of 1.0 eV was reported. This branch is shown as a gray band in Figure 6 and can be reproduced using a heating and cooling routine where the temperature is progressively raised.[32] This phenomenon, along with anomalies in magnetic susceptibility and charge distribution data, were argued by Batllo and co-workers[34] to arise from the disassociation of holes bound to doubly negative Mg vacancies. These hole−vacancy complexes are created by the incorporation of trace H_2O during crystal growth and are thus of extrinsic origin.[34] The holes were postulated to be localized on the oxygen sublattice, which would make them very similar to the small hole polarons identified in the present study. Taken together, these observations suggest that the conduction mechanism in the 1 eV branch is the dissociative formation, and subsequent migration, of p^+.

To test this hypothesis we calculated the disassociation energy of a single p^+ bound within a $2p^+$−V_{Mg}^{2-} complex:[33]

$$(p^{2+}\, V_{Mg}^{2-})^x \rightleftharpoons (p^+\, V_{Mg}^{2-})^- + p^+ \tag{7}$$

Reaction 7 may be followed by the dissociation of the remaining p^+, per

$$(p^+\, V_{Mg}^{2-})^- \rightleftharpoons V_{Mg}^{2-} + p^+ \tag{8}$$

The calculated p^+ disassociation energies (eqs 7 and 8) are similar, 0.87 and 0.85 eV, respectively. Taking these dissociation energies as an effective formation energy and combining them with the polaron migration energy, we derive a calculated Arrhenius energy of 0.97 eV. This value is in remarkable agreement with the measured value of 1.0 eV, resulting in the similar slopes for the calculated (gray line) and measured (gray oval) data shown in Figure 6. This observation supports the hypothesis that the 1 eV branch is due to the liberation and migration of p+ bound to negative vacancies. (Because the carriers in this branch are extrinsic in origin and their concentration is not well-established, the calculated Arrhenius branch in Figure 6 has been positioned (vertically) using the measured conductivity.[32] Therefore, the most meaningful comparison between theory and experiment in this branch is the Arrhenius energy.)

IV. CONCLUSIONS

We have presented a comprehensive analysis of charge transport mechanisms within the primary discharge products, MgO and MgO_2, of an Mg/O_2 battery. While these batteries have extremely high theoretical energy densities, their benefits have yet to be realized in a practical cell that is both reversible and long-lived. Understanding transport within the nominally insulating discharge phases is an important step toward overcoming these performance gaps.

In the case of MgO, our calculations identify doubly negative Mg vacancies and hole polarons as the dominant charge carriers. For MgO_2, electronic charge carriers alone—electron

DOI: 10.1021/acs.chemmater.7b00217
Chem. Mater. XXXX, XXX, XXX−XXX

and hole polarons—are the most prevalent. Due to the large formation energies associated with defects in both compounds, the equilibrium concentration of charge carriers is predicted to be low at the near-ambient temperatures expected for battery operation. These low concentrations also offset the moderate (for MgO_2) to high (in MgO) mobility of hole polarons. Consequently, if *equilibrium* carrier concentrations are realized, the conductivity for both MgO and MgO_2 will be low and thus likely limit battery performance.

Nevertheless, charge transport within the discharge products of a realistic battery cathode will be strongly influenced by *nonequilibrium* effects. These effects arise from fast growth rates during discharge, impurity incorporation from the electrolyte, and limited ion mobility at ambient temperatures. In combination with the moderate/high mobilities predicted for hole polarons, these nonequilibrium effects suggest a strategy for improving conductivity: artificially increasing polaron concentrations via the incorporation of monovalent impurities into the discharge product during its growth. In principle, this could be achieved through the intentional addition of small quantities of lithium ions to the electrolyte.

Finally, the calculated conductivity data for MgO are observed to be in remarkable agreement with the three Arrhenius branches reported in experiments and thus clarify the long-debated transport mechanisms within these regimes.

AUTHOR INFORMATION

Corresponding Author

*(D.J.S.) E-mail: djsiege@umich.edu. Phone: 734-764-4808.

ORCID

Jeffrey G. Smith: 0000-0002-0613-8057

Donald J. Siegel: 0000-0001-7913-2513

Notes

The authors declare no competing financial interest.

ACKNOWLEDGMENTS

J.G.S. and D.J.S. gratefully acknowledge financial support from DENSO Corporation. D.J.S. acknowledges DTU Energy, the Villum Foundation's Visiting Professor Program, and the Nordea Foundation's Residence Program for support during his stay at DTU. J.G.S. acknowledges partial support from the National Science Foundation, Grant CBET-1336387.

REFERENCES

(1) Girishkumar, G.; McCloskey, B.; Luntz, A. C.; Swanson, S.; Wilcke, W. Lithium−Air Battery: Promise and Challenges. *J. Phys. Chem. Lett.* **2010**, *1*, 2193−2203.

(2) Imanishi, N.; Luntz, A.; Bruce, P. *The Lithium Air Battery: Fundamentals*; Springer: New York, 2014.

(3) Radin, M. D.; Siegel, D. J. Non-Aqueous Metal-Air Batteries: Past, Present, and Future. In *Rechargeable Batteries: Materials, Technologies and New Trends*; Zhang, Z., Zhang, S. S., Eds.; Springer: 2015; pp 511−539.

(4) Bruce, P. G.; Freunberger, S. A.; Hardwick, L. J.; Tarascon, J.-M. Li-O2 and Li-S Batteries with High Energy Storage. *Nat. Mater.* **2012**, *11*, 19−29.

(5) Christensen, J.; Albertus, P.; Sanchez-Carrera, R. S.; Lohmann, T.; Kozinsky, B.; Liedtke, R.; Ahmed, J.; Kojic, A. A Critical Review of Li/Air Batteries. *J. Electrochem. Soc.* **2012**, *159*, R1−R30.

(6) Aurbach, D.; Lu, Z.; Schechter, A.; Gofer, Y.; Gizbar, H.; Turgeman, R.; Cohen, Y.; Moshkovich, M.; Levi, E. Prototype Systems for Rechargeable Magnesium Batteries. *Nature* **2000**, *407*, 724−727.

(7) Muldoon, J.; Bucur, C. B.; Oliver, A. G.; Sugimoto, T.; Matsui, M.; Kim, H. S.; Allred, G. D.; Zajicek, J.; Kotani, Y. Electrolyte Roadblocks to a Magnesium Rechargeable Battery. *Energy Environ. Sci.* **2012**, *5*, 5941−5950.

(8) Chase, M. W. *NIST-JANAF Thermochemical Tables*, 4th ed.; American Institute of Physics: 1998.

(9) Smith, J. G.; Naruse, J.; Hiramatsu, H.; Siegel, D. J. Theoretical Limiting Potentials in Mg/O2 Batteries. *Chem. Mater.* **2016**, *28*, 1390−1401.

(10) Shiga, T.; Hase, Y.; Kato, Y.; Inoue, M.; Takechi, K. A Rechargeable Non-Aqueous Mg-O2 Battery. *Chem. Commun.* **2013**, *49*, 9152−9154.

(11) Shiga, T.; Hase, Y.; Yagi, Y.; Takahashi, N.; Takechi, K. Catalytic Cycle Employing a TEMPO − Anion Complex to Obtain a Secondary Mg − O2 Battery. *J. Phys. Chem. Lett.* **2014**, *5*, 1648−1652.

(12) Vardar, G.; Nelson, E. G.; Smith, J. G.; Naruse, J.; Hiramatsu, H.; Bartlett, B. M.; Sleightholme, A. E. S.; Siegel, D. J.; Monroe, C. W. Identifying the Discharge Product and Reaction Pathway for a Secondary Mg/O2 Battery. *Chem. Mater.* **2015**, *27*, 7564−7568.

(13) Vardar, G.; Smith, J. G.; Thompson, T.; Inagaki, K.; Naruse, J.; Hiramatsu, H.; Sleightholme, A. E. S.; Sakamoto, J.; Siegel, D. J.; Monroe, C. W. A Mg/O2 Battery Based on the MACC Electrolyte. *Chem. Mater.* **2016**, *28*, 7629−7637.

(14) Garcia-Lastra, J. M.; Myrdal, J. S. G.; Christensen, R.; Thygesen, K. S.; Vegge, T. DFT+U Study of Polaronic Conduction in Li2O2 and Li2CO3: Implications for Li-Air Batteries. *J. Phys. Chem. C* **2013**, *117*, 5568−5577.

(15) Radin, M. D.; Siegel, D. J. Charge Transport in Lithium Peroxide: Relevance for Rechargeable Metal−air Batteries. *Energy Environ. Sci.* **2013**, *6*, 2370−2379.

(16) Radin, M. D.; Monroe, C. W.; Siegel, D. J. Impact of Space-Charge Layers on Sudden Death in Li/O2 Batteries. *J. Phys. Chem. Lett.* **2015**, *6*, 3017−3022.

(17) Radin, M. D.; Monroe, C. W.; Siegel, D. J. How Dopants Can Enhance Charge Transport in Li2O2. *Chem. Mater.* **2015**, *27*, 839−847.

(18) Tian, F.; Radin, M. D.; Siegel, D. J. Enhanced Charge Transport in Amorphous Li2O2. *Chem. Mater.* **2014**, *26*, 2952−2959.

(19) Radin, M. D.; Tian, F.; Siegel, D. J. Electronic Structure of Li2O2 {0001} Surfaces. *J. Mater. Sci.* **2012**, *47*, 7564−7570.

(20) Radin, M. D.; Rodriguez, J. F.; Tian, F.; Siegel, D. J. Lithium Peroxide Surfaces Are Metallic, While Lithium Oxide Surfaces Are Not. *J. Am. Chem. Soc.* **2012**, *134*, 1093−1103.

(21) Lempicki, A. The Electrical Conductivity of MgO Single Crystals at High Temperatures. *Proc. Phys. Soc., London, Sect. B* **1953**, *66*, 281−283.

(22) Mansfield, R. The Electrical Conductivity and Thermoelectric Power of Magnesium Oxide. *Proc. Phys. Soc., London, Sect. B* **1953**, *66*, 612−614.

(23) Yamaka, E.; Sawamoto, K. Electrical Conductivity and Thermo-Electric Motive Force in MgO Single Crystal. *J. Phys. Soc. Jpn.* **1955**, *10*, 176−179.

(24) Mitoff, S. P. Electrical Conductivity of Single Crystals of MgO. *J. Chem. Phys.* **1959**, *31*, 1261−1269.

(25) Mitoff, S. P. Electronic and Ionic Conductivity in Single Crystals of MgO. *J. Chem. Phys.* **1962**, *36*, 1383−1389.

(26) Davies, M. O. Transport Phenomena in Pure and Doped Magnesium Oxide. *J. Chem. Phys.* **1963**, *38*, 2047−2055.

(27) Lewis, T. J.; Wright, R. W. The Electrical Conductivity of Magnesium Oxide at Low Temperatures. *J. Phys. D: Appl. Phys.* **1968**, *1*, 441−447.

(28) Osburn, C. M.; Vest, R. W. Electrical Properties of Single Crystals, Bicrystals, and Polycrystals of MgO. *J. Am. Ceram. Soc.* **1971**, *54*, 428−435.

(29) Sempolinski, D. R.; Kingery, W. D. Ionic Conductivity and Magnesium Vacancy Mobility in Magnesium Oxide. *J. Am. Ceram. Soc.* **1980**, *63*, 664−669.

(30) Sempolinski, D. R.; Kingery, W. D.; Tuller, H. L. Electronic Conductivity of Single Crystalline Magnesium Oxide. *J. Am. Ceram. Soc.* **1980**, *63*, 669−675.

DOI: 10.1021/acs.chemmater.7b00217
Chem. Mater. XXXX, XXX, XXX−XXX

(31) Kathrein, H.; Knipping, U.; Freund, F. Atomic Carbon in Magnesium Oxide, Part VI, Electrical Conductivity. *Mater. Res. Bull.* **1980**, *15*, 1393−1399.
(32) Kathrein, H.; Freund, F. Electrical Conductivity of Magnesium Oxide Single Crystal below 1200 K. *J. Phys. Chem. Solids* **1983**, *44*, 177−186.
(33) Freund, F.; Freund, M.; Batllo, F. Critical Review of Electrical Conductivity Measurements and Charge Distribution Analysis of Magnesium Oxide. *J. Geophys. Res.* **1993**, *98*, 22209−22229.
(34) Batllo, F.; Leroy, R. C.; Parvin, K.; Freund, F. Dissociation of O2−2 Defects into Paramagnetic O- in Wide Band-Gap Insulators: A Magnetic Susceptibility Study of Magnesium Oxide. *J. Appl. Phys.* **1990**, *67*, 5844−5846.
(35) Batllo, F.; Leroy, R. C.; Parvin, K.; Freund, F.; Freund, M. M. Positive Holes in Magnesium Oxide. Correlation between Magnetic, Electric, and Dielectric Anomalies. *J. Appl. Phys.* **1991**, *69*, 6031−6033.
(36) Catlow, C. R. A.; Faux, I. D.; Norgett, M. J. Shell and Breathing Shell Model Calculations for Defect Formation Energies and Volumes in Magnesium Oxide. *J. Phys. C: Solid State Phys.* **1976**, *9*, 419−430.
(37) Mackrodt, W. C.; Stewart, R. F. Defect Properties of Ionic Solids. II. Point Defect Energies Based on Modified Electron-Gas Potentials. *J. Phys. C: Solid State Phys.* **1979**, *12*, 431−449.
(38) Mackrodt, W. C.; Stewart, R. F. Defect Properties of Ionic Solids. III. The Calculation of the Point-Defect Structure of the Alkaline-Earth Oxides and CdO. *J. Phys. C: Solid State Phys.* **1979**, *12*, 5015−5036.
(39) Sangster, M. J. L.; Rowell, D. K. Calculation of Defect Energies and Volumes in Some Oxides. *Philos. Mag. A* **1981**, *44*, 613−624.
(40) Grimes, R. W.; Catlow, C. R. A. Modeling Localized Defects in Ionic Materials Using Mott-Littleton and Embedded Quantum Cluster Methodology. *J. Am. Ceram. Soc.* **1990**, *73*, 3251−3256.
(41) De Vita, A.; Gillan, M. J.; Lin, J. S.; Payne, M. C.; Stich, I.; Clarke, L. J. Defect Energetics in MgO Treated by First-Principles Methods. *Phys. Rev. B: Condens. Matter Mater. Phys.* **1992**, *46*, 12964−12973.
(42) Vočadlo, L.; Wall, A.; Parker, S. C.; Price, G. D. Absolute Ionic Diffusion in MgO-Computer Calculations via Lattice Dynamics. *Phys. Earth Planet. Inter.* **1995**, *88*, 193−210.
(43) Busker, G.; Van Huis, M. A.; Grimes, R. W.; Van Veen, A. Predicted Vacancy Cluster Structures in MgO and Their Interaction with Helium. *Nucl. Instrum. Methods Phys. Res., Sect. B* **2000**, *171*, 528−536.
(44) Alfè, D.; Gillan, M. J. Schottky Defect Formation Energy in MgO Calculated by Diffusion Monte Carlo. *Phys. Rev. B: Condens. Matter Mater. Phys.* **2005**, *71*, 220101.
(45) Uberuaga, B. P.; Smith, R.; Cleave, A. R.; Henkelman, G.; Grimes, R. W.; Voter, A. F.; Sickafus, K. E. Dynamical Simulations of Radiation Damage and Defect Mobility in MgO. *Phys. Rev. B: Condens. Matter Mater. Phys.* **2005**, *71*, 104102.
(46) Gilbert, C. A.; Kenny, S. D.; Smith, R.; Sanville, E. Ab Initio Study of Point Defects in Magnesium Oxide. *Phys. Rev. B: Condens. Matter Mater. Phys.* **2007**, *76*, 184103.
(47) Runevall, O.; Sandberg, N. Self-Diffusion in MgO—a Density Functional Study. *J. Phys.: Condens. Matter* **2011**, *23*, 345402.
(48) Mulroue, J.; Duffy, D. An Ab Initio Study of the Effect of Charge Localization on Oxygen Defect Formation and Migration Energies in Magnesium Oxide. *Proc. R. Soc. London, Ser. A* **2011**, *467*, 2054−2065.
(49) Grüneis, A. Efficient Explicitly Correlated Many-Electron Perturbation Theory for Solids: Application to the Schottky Defect in MgO. *Phys. Rev. Lett.* **2015**, *115*, 066402.
(50) Kang, J.; Jung, Y. S.; Wei, S.-H.; Dillon, A. C. Implications of the Formation of Small Polarons in Li2O2 for Li-Air Batteries. *Phys. Rev. B: Condens. Matter Mater. Phys.* **2012**, *85*, 035210.
(51) Ong, S. P.; Mo, Y.; Ceder, G. Low Hole Polaron Migration Barrier in Lithium Peroxide. *Phys. Rev. B: Condens. Matter Mater. Phys.* **2012**, *85*, 081105.
(52) Gerbig, O.; Merkle, R.; Maier, J. Electron and Ion Transport in Li2O2. *Adv. Mater.* **2013**, *25*, 3129−3133.
(53) Lu, Y.-C.; Kwabi, D. G.; Yao, K. P. C.; Harding, J. R.; Zhou, J.; Zuin, L.; Shao-Horn, Y. The Discharge Rate Capability of Rechargeable Li−O2 Batteries. *Energy Environ. Sci.* **2011**, *4*, 2999−3007.
(54) Timoshevskii, V.; Feng, Z.; Bevan, K. H.; Goodenough, J.; Zaghib, K. Improving Li2O2 Conductivity via Polaron Preemption: An Ab Initio Study of Si Doping. *Appl. Phys. Lett.* **2013**, *103*, 073901.
(55) Araujo, R. B.; Chakraborty, S.; Ahuja, R. Unveiling the Charge Migration Mechanism in Na2O2: Implications for Sodium−air Batteries. *Phys. Chem. Chem. Phys.* **2015**, *17*, 8203−8209.
(56) Yang, S.; Siegel, D. J. Intrinsic Conductivity in Sodium−Air Battery Discharge Phases: Sodium Superoxide vs Sodium Peroxide. *Chem. Mater.* **2015**, *27*, 3852−3860.
(57) Gerbig, O.; Merkle, R.; Maier, J. Electrical Transport and Oxygen Exchange in the Superoxides of Potassium, Rubidium, and Cesium. *Adv. Funct. Mater.* **2015**, *25*, 2552−2563.
(58) Viswanathan, V.; Thygesen, K. S.; Hummelshøj, J. S.; Nørskov, J. K.; Girishkumar, G.; McCloskey, B. D.; Luntz, A. C. Electrical Conductivity in Li 2 O 2 and Its Role in Determining Capacity Limitations in Non-Aqueous Li-O 2 Batteries. *J. Chem. Phys.* **2011**, *135*, 214704.
(59) Lee, B.; Kim, J.; Yoon, G.; Lim, H. D.; Choi, I. S.; Kang, K. Theoretical Evidence for Low Charging Overpotentials of Superoxide Discharge Products in Metal-Oxygen Batteries. *Chem. Mater.* **2015**, *27*, 8406−8413.
(60) Sasaki, K.; Maier, J. Low-Temperature Defect Chemistry of Oxides. I. General Aspects and Numerical Calculations. *J. Appl. Phys.* **1999**, *86*, 5422−5433.
(61) Maier, J. Complex Oxides: High Temperature Defect Chemistry vs. Low Temperature Defect Chemistry. *Phys. Chem. Chem. Phys.* **2003**, *5*, 2164−2173.
(62) Maier, J. High Temperature versus Low Temperature Defect Chemistry. *Solid State Ionics* **2004**, *173*, 1−8.
(63) Whittingham, M. S. Lithium Batteries and Cathode Materials. *Chem. Rev.* **2004**, *104*, 4271−4301.
(64) Sheppard, D.; Terrell, R.; Henkelman, G. Optimization Methods for Finding Minimum Energy Paths. *J. Chem. Phys.* **2008**, *128*, 134106.
(65) Henkelman, G.; Jónsson, H. Improved Tangent Estimate in the Nudged Elastic Band Method for Finding Minimum Energy Paths and Saddle Points. *J. Chem. Phys.* **2000**, *113*, 9978−9985.
(66) Henkelman, G.; Uberuaga, B. P.; Jónsson, H. A Climbing Image Nudged Elastic Band Method for Finding Saddle Points and Minimum Energy Paths. *J. Chem. Phys.* **2000**, *113*, 9901−9904.
(67) Kresse, G.; Furthmuller, J. Efficiency of Ab-Initio Total Energy Calculations for Metals and Semiconductors Using a Plane-Wave Basis Set. *Comput. Mater. Sci.* **1996**, *6*, 15−50.
(68) Kresse, G.; Hafner, J. Ab Initio Molecular Dynamics for Liquid Metals. *Phys. Rev. B: Condens. Matter Mater. Phys.* **1993**, *47*, 558−561.
(69) Kresse, G.; Hafner, J. Ab Initio Molecular-Dynamics Simulation of the Liquid-Metal-Amorphous-Semiconductor Transition in Germanium. *Phys. Rev. B: Condens. Matter Mater. Phys.* **1994**, *49*, 14251−14269.
(70) Kresse, G.; Furthmüller, J. Efficient Iterative Schemes for Ab Initio Total-Energy Calculations Using a Plane-Wave Basis Set. *Phys. Rev. B: Condens. Matter Mater. Phys.* **1996**, *54*, 11169−11186.
(71) Blochl, P. E. Projector Augmented-Wave Method. *Phys. Rev. B: Condens. Matter Mater. Phys.* **1994**, *50*, 17953−17979.
(72) Shishkin, M.; Kresse, G. Implementation and Performance of the Frequency-Dependent GW Method within the PAW Framework. *Phys. Rev. B: Condens. Matter Mater. Phys.* **2006**, *74*, 035101.
(73) Shishkin, M.; Marsman, M.; Kresse, G. Accurate Quasiparticle Spectra from Self-Consistent GW Calculations with Vertex Corrections. *Phys. Rev. Lett.* **2007**, *99*, 246403.
(74) Heyd, J.; Scuseria, G. E.; Ernzerhof, M. Hybrid Functionals Based on a Screened Coulomb Potential. *J. Chem. Phys.* **2003**, *118*, 8207−8215.

DOI: 10.1021/acs.chemmater.7b00217
Chem. Mater. XXXX, XXX, XXX−XXX

(75) Krukau, A. V.; Vydrov, O. a; Izmaylov, A. F.; Scuseria, G. E. Influence of the Exchange Screening Parameter on the Performance of Screened Hybrid Functionals. *J. Chem. Phys.* **2006**, *125*, 224106.
(76) Makov, G.; Payne, M. C. Periodic Boundary Conditions in Ab Initio Calculations. *Phys. Rev. B: Condens. Matter Mater. Phys.* **1995**, *51*, 4014−4022.
(77) Komsa, H.-P.; Rantala, T. T.; Pasquarello, A. Finite-Size Supercell Correction Schemes for Charged Defect Calculations. *Phys. Rev. B: Condens. Matter Mater. Phys.* **2012**, *86*, 045112.
(78) Gajdoš, M.; Hummer, K.; Kresse, G.; Furthmüller, J.; Bechstedt, F. Linear Optical Properties in the Projector-Augmented Wave Methodology. *Phys. Rev. B: Condens. Matter Mater. Phys.* **2006**, *73*, 045112.
(79) Wang, L.; Maxisch, T.; Ceder, G. Oxidation Energies of Transition Metal Oxides within the GGA+U Framework. *Phys. Rev. B: Condens. Matter Mater. Phys.* **2006**, *73*, 195107.
(80) Van de Walle, C. G.; Neugebauer, J. First-Principles Calculations for Defects and Impurities: Applications to III-Nitrides. *J. Appl. Phys.* **2004**, *95*, 3851−3879.
(81) Lidiard, A. *Handbook of Physics*; Flugge, S., Ed.; Springer-Verlag: Berlin, 1957.
(82) Tilley, R. J. D. *Defects in Solids*; John Wiley & Sons, Inc.: 2008.
(83) Smith, D. K.; Leider, H. R. Low-Temperature Thermal Expansion of LiH, MgO and CaO. *J. Appl. Crystallogr.* **1968**, *1*, 246−249.
(84) Vannerberg, N. The Formation and Structure of Magnesium Peroxide. *Ark. Kemi* **1959**, *14*, 99−105.
(85) Shishkin, M.; Kresse, G. Self-Consistent GW Calculations for Semiconductors and Insulators. *Phys. Rev. B: Condens. Matter Mater. Phys.* **2007**, *75*, 235102.
(86) Whited, R. C.; Flaten, C. J.; Walker, W. C. Exciton Thermoreflectance of MgO and CaO. *Solid State Commun.* **1973**, *13*, 1903−1905.
(87) Sproul, A. B.; Green, M. A.; Zhao, J. Improved Value for the Silicon Intrinsic Carrier Concentration at 300 K. *Appl. Phys. Lett.* **1990**, *57*, 255−257.
(88) Freund, M. M.; Freund, F.; Batllo, F. Highly Mobile Oxygen Holes in Magnesium Oxide. *Phys. Rev. Lett.* **1989**, *63*, 2096−2099.
(89) Mackrodt, W. C. Defect Calculations for Ionic Materials. In *Computer Simulation of Solids*; Mackrodt, W. C., Catlow, C. R. A., Eds.; Springer-Verlag: Berlin, 1982; p 175.
(90) Vol'nov, I. I.; Tokareva, S. A.; Belevskii, V. N.; Latysheva, E. I. The Formation of Magnesium Perperoxide in the Reaction of Magnesium Peroxide with Ozone. *Bull. Acad. Sci. USSR, Div. Chem. Sci.* **1970**, *19* (3), 468−471.
(91) Sangster, M. J. L.; Peckham, G.; Saunderson, D. H. Lattice Dynamics of Magnesium Oxide. *J. Phys. C: Solid State Phys.* **1970**, *3*, 1026.
(92) Masetti, G.; Severi, M.; Solmi, S. Modeling of Carrier Mobility Against Carrier Concentration in Arsenic-, Phosphorus-, and Boron-Doped Silicon. *IEEE Trans. Electron Devices* **1983**, *30*, 764−769.
(93) Kroger, F. A.; Vink, H. J. Relations between the Concentrations of Imperfections in Crystalline Solids. *Solid State Phys.* **1956**, *3*, 307−435.
(94) Kroger, F. A. *The Chemistry of Imperfect Crystals*; North-Holland Publishing Company: Amsterdam, 1964.
(95) Chen, Y.; Kernohan, R. H.; Boldu, J. L.; Abraham, M.; Eisenberg, D. J.; Crawford, J. H., Jr. Enhancement of Electrical Conductivity in MgO Due to Lithium Impurities. *Solid State Commun.* **1980**, *33*, 441−443.
(96) Tardío, M.; Ramírez, R.; González, R.; Pinto, J. V.; Da Silva, R. C.; Alves, E.; Chen, Y. Electrical Conductivity of as-Grown and Oxidized MgO:Li Crystals Implanted with Li Ions. *Nucl. Instrum. Methods Phys. Res., Sect. B* **2004**, *218*, 164−169.
(97) Jost, W. Ion-Disorder Energies and Mobility in Crystals. *Phys. Zeitschrift* **1935**, *36*, 757−760.
(98) Strehlow, W. H.; Cook, E. L. Compilation of Energy Band Gaps in Elemental and Binary Compound Semiconductors and Insulators. *J. Phys. Chem. Ref. Data* **1973**, *2*, 163−200.

DOI: 10.1021/acs.chemmater.7b00217
Chem. Mater. XXXX, XXX, XXX−XXX